Reprinted from
Journal of Imaging Science and Technology® 63(4): 040403-1–040403-8, 2019.

The Effect of Subsurface Structure on the Color Appearance of 3D Printed Objects

Matt Ronnenberg▲ **and Susan Farnand**▲
Rochester Institute of Technology, Rochester, NY
E-mail: mxr8103@rit.edu

Abstract. *Relatively recent advancements in 3D printing include the ability to print with multiple materials and in multiple colors. Traditional 2D printers, which print to flat media, assume that the surface geometry has a negligible effect on the appearance. The International Color Consortium (ICC) builds profiles allowing for color communication among devices, including traditional 2D printers. The ICC does not currently have practices in place to build profiles for color 3D printers due, in part, to several unknown parameters affecting the appearance of 3D printed objects. One such unknown parameter is the surface structure. To test the effect of surface structure on the color appearance of 3D printed objects, 3D models were built digitally with goniochromatic effects in mind and then printed using a color 3D printer. Spectral radiance and bidirectional reflectance distribution function measurements of the 3D printed samples were taken and correlated with the results of a psychophysical experiment to test for changes in the appearance. It was found that surface structure does have a measurable, perceptible effect on the color appearance of 3D printed objects.*

[DOI: 10.2352/J.ImagingSci.Technol.2019.63.4.040403]

1. INTRODUCTION

A study conducted by Domingue et al. attempted to fabricate female emerald ash borers, an invasive species of beetle with an iridescent appearance, with enough accuracy to attract male beetles [1]. The decoy beetles were connected to a battery and males that landed on them were killed as an alert to the presence of the beetles and as part of an overall eradication program. Decoy beetles were produced using several techniques, one of which was 3D printing. The printed decoys were painted with metallic paint in an attempt to mimic the iridescent appearance of living beetles, while the other decoys were colored using different methods. Of all the beetle decoys used in this study, the 3D printed decoy produced the weakest results. The primary issue with the 3D printed decoy was that it was highly reflective due to the metallic paint, but it did not produce a strong goniochromatic effect. This study served as the inspiration for the current project.

What would later become known as 3D printing began as a technology called stereolithography, first patented by Charles Hull in 1986 [2]. The original idea was to add materials layer by layer until the desired shape was achieved. This concept has evolved over the years and now encompasses several techniques which could fall under the category of 3D printing [3]. As these technologies continue to develop and become increasingly affordable, the range of available materials and applications is expected to grow.

Along with new applications will come new challenges, one of which is how to print individual objects with multiple colors. Traditionally, most 3D printers have only been capable of printing a specific material in one color at a time. This is changing as the number and quality of 3D printers able to print multiple colors in a single assembly is increasing. Other studies have already begun developing techniques to improve color uniformity and appearance quality in 3D printing [4–6].

The International Color Consortium (ICC) is an organization that sets standards with regard to color communications between devices. ICC profiles are used to translate color data created on one device to another device's native color space [7]. For example, an image captured by a smartphone's RGB camera can be sent to a printer which prints using cyan, magenta, yellow and black (CMYK) primaries. Without some type of color management, such as ICC profiles defined for both the camera and the printer, the printed image would be unlikely to accurately reproduce colors found in the original scene.

With the introduction of a new ICC specification, iccMAX, parameters affected by surface and subsurface structure, such as bidirectional reflectance distribution function (BRDF), can be used to build ICC profiles [8]. The previous work funded by the ICC used BRDF measurements of real objects and the Blinn–Phong and Cook–Torrance models to simulate color appearance using iccMAX [9]. Another work has also been done to optimize uniformity of surface appearance for color 3D printed objects, though that study did not take the effect of non-uniformity along surfaces into account [10]. Profiling and calibrating 2D printers is done by measuring uniform color patches. However, this would not be practical for 3D objects since complex scenes cannot be represented by images with reduced dimensionality [11]. It is therefore necessary to define the required parameters for profiling printers capable of producing objects with complex appearance properties. The current project aims to explore parameters known to affect appearance, primarily goniochromatic properties, to

▲ IS&T Members.

Received Mar. 12, 2019; accepted for publication July 4, 2019; published online Aug. 22, 2019. Associate Editor: Marius Pedersen.
1062-3701/2019/63(4)/040403/8/$25.00

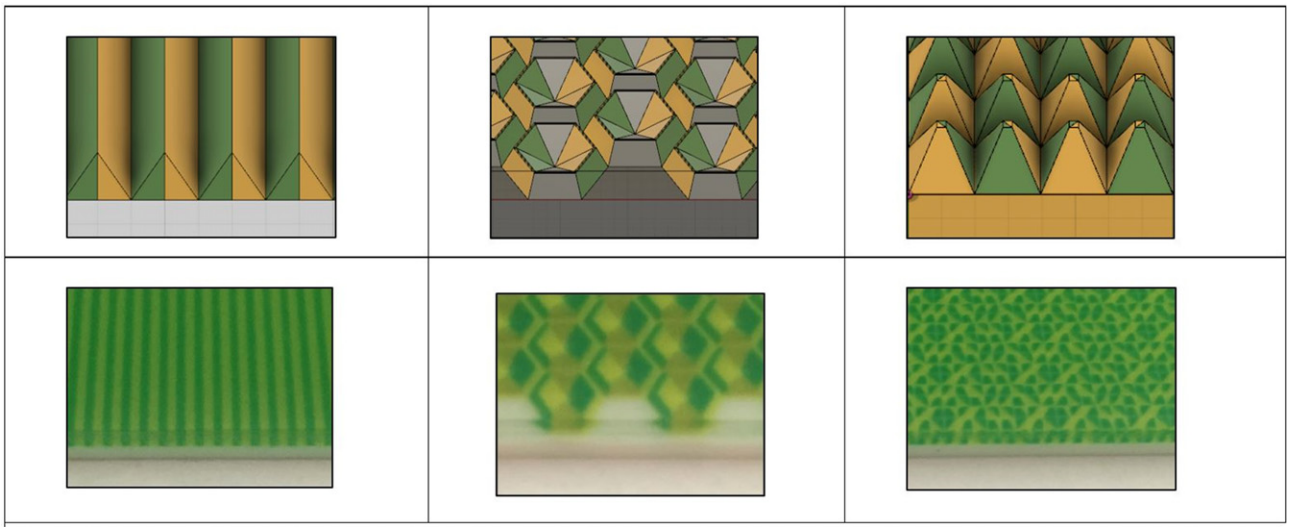

Figure 1. Top row: Objects modeled in Autodesk® Fusion 360. Bottom row: Same objects printed using a Stratasys® J750 3D printer. Modeled samples are not intended to match the color of printed samples as the Autodesk® Fusion 360 color palette was limited. They are simply an illustration. Samples, starting from the left, are referred to as ''tent,'' ''honeycomb'' and ''pyramid'' after the shape of the geometries used.

later determine which dimensions are necessary to define a color appearance gamut for 3D objects in future work.

The challenge in reproducing goniochromatic effects, such as the iridescent appearance of beetles, using modern 3D printers is that the minimum size printers can achieve is restricted by the minimum size of materials used. The printer used in this study, a Stratasys® J750, can print details as small as 0.014 mm [12]. This printer uses a PolyJet printing process, which works by applying an extremely thin layer of photopolymer and then curing with UV bulbs [13]. While printing a 3D object on a micro-scale in multiple specified colors is impressive, it is still too large a scale to reproduce iridescence, which is the result of constructive and destructive interference of light caused by physical nano-scale surface structures. While interference cannot be truly replicated by present day 3D printers, comparable goniochromatic effects may still be mimicked by varying the surface structure of objects printed in multiple colors.

Some details of the current study were reported in the authors' previous work [14]. That study focused primarily on color measurement of 3D printed objects to see if goniochromatic effects were possible. While measurements are again reported here, the primary focus of this study is to validate those measurements with a psychophysical experiment using human observers.

2. METHODS

In order to study goniochromatic effects, 3D printed objects with flat surfaces and varying subsurface structures were produced. 3D renderings were first created using Autodesk® Fusion 360 software. The renderings each had different geometries modeled on a white base, which were then covered by several layers of transparent material. This resulted in samples with a flat surface but non-uniform 3D structures.

Table I. Example CIELAB values from measurements of an emerald ash borer.

	Elytra	Eye	Side	Belly
L^*	22.83	40.62	21.46	26.19
a^*	−9.08	−22.13	−12.31	−4.68
b^*	10.30	22.39	11.47	8.30

The renderings, shown in the top row of Figure 1, were sent to Stratasys® Direct Manufacturing where they were printed using a Stratasys® J750 3D printer. Three such models have been designed and printed. Designing and printing more samples would have been ideal but was not possible due to financial constraints. Color custom 3D printing is still relatively expensive. Most 3D printers can only print one color at a time, but the Stratasys® J750 can print multiple colors on a single part using cyan, magenta, yellow, black and white primaries. These are detailed in the Polyjet Color Materials guide which was provided by Stratasys® [15]. The colors selected were inspired by the CIELAB values of emerald ash borers, which were calculated from measurements of an emerald ash borer carcass taken with a PR 740 spectroradiometer under two LED lights, each at 45° from either side of the ash borers (Table I) [7, 16].

Measurements were taken for multiple parts of the beetle including the eye, belly, side and elytra. Elytra are solid protective wing casings and can be seen in Figure 2 running the full length of the beetle's back. The measurements taken from the beetles themselves were relatively low chroma. Visual inspection of the beetle and the desire for a measurable goniochromatic effect were also taken into account when deciding on the Polyjet colors to use. In the end, green and yellow colors were chosen as they most closely matched the beetle's emerald green and gold appearance. Table II

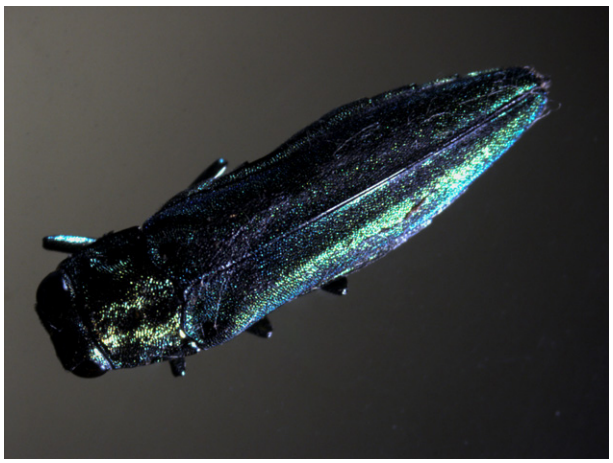

Figure 2. Micro-graph image of an emerald ash borer.

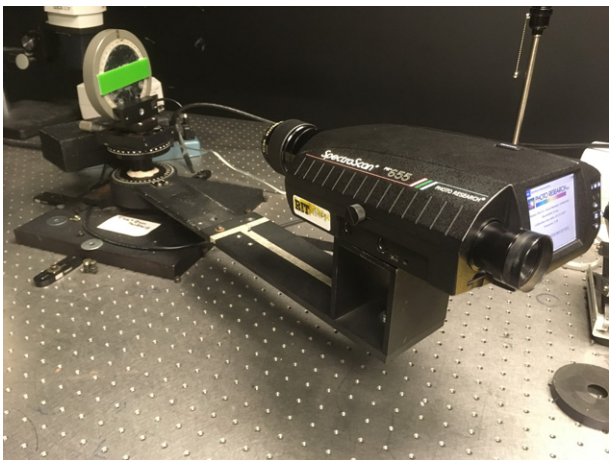

Figure 3. Gonio-arm setup.

Table II. CIELAB values of materials used in 3D prints taken from Stratasys® PolyJet Color Guide.

	RGD-CY-003	VeroYellow	RGD-CMY-012
L^*	37.52	71.12	46.64
a^*	−37.28	−2.03	−11.48
b^*	25.95	90.24	50.87

lists the CIELAB values of the materials used for the final prints. Unfortunately, no further information was provided by Stratasys® regarding the methods used to acquire the Polyjet CIELAB values. However, the differences of the beetle and the closest Polyjet materials are substantial.

2.1 *Measurements*

Note that a third color, RGD-CMY-012, was used only for the "honeycomb" sample as a transitionary color. The CIEDE2000 color difference was calculated for RGD-CY-003 and VeroYellow. The differences between these two colors and several others from the Polyjet Color Guide were then calculated in order to choose a third color that would lie closest to the perceptual center.

Radiance measurements were taken using a PR-655 SpectraScan spectroradiometer. Each sample was placed on a stationary stand while the PR-655 was mounted onto a rotating arm in front of it, as shown in Figure 3. The light source was placed behind and above the PR-655 and faced directly toward the samples at an angle of approximately 45°. The light source remained stationary during all measurements so that only the angle of observation was varied. Measurements were taken at every 5° up to 80° outward on either side of the sample's surface normal.

BRDF measurements were taken using a Murakami goniospectrophotometer, shown with one of the printed samples placed inside in Figure 4. BRDF measurements are important for characterizing object appearance due to the effect non-uniform 3D geometry can have on appearance. This device allows for precise, automated

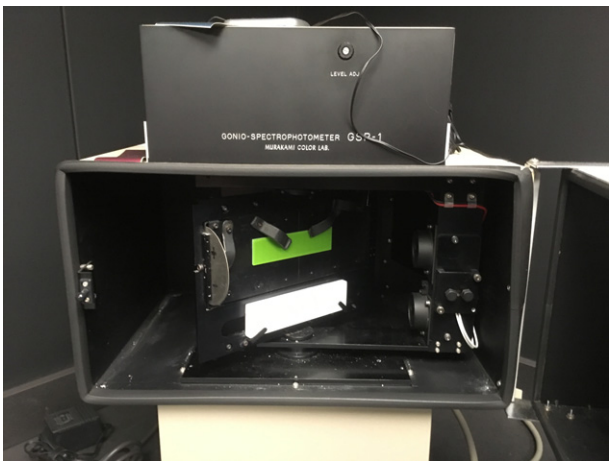

Figure 4. Sample inside Murakami goniospectrophotometer.

measurements while varying both angle of incidence and angle of observation. The angle of incidence ranged from 0° to 75° in steps of 15°, while the angle of observation ranged from 0° to 75° in steps of 5°, or 2° if close to the specular angle. The reflectance measurements taken with the goniospectrophotometer were used to calculate CIE XYZ tristimulus values and CIELAB using D65 as the reference white point [7, 16].

2.2 *Perceptual Testing*

Figure 5 shows the tent sample from both sides. In these images, one side appears greener and the other yellower. While this is apparent from the extremes, gradual changes in color appearance should occur as the objects are rotated from the center. Perceptual testing will determine how those changes are seen by observers.

Goniochromatic measurements do not guarantee a change in color appearance. A psychophysical experiment was conducted as a means of verifying the color measurements with human observers [17]. Each sample was imaged from 70° on one side to 70° on the other in steps of 10°. The images were taken with a Fujifilm® XT100 digital camera, which was manually white balanced using an X-Rite®

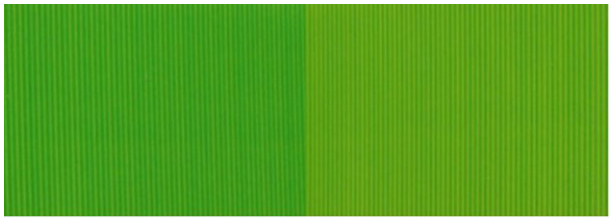

Figure 5. Tent sample viewed at 55° from surface normal on both sides.

ColorChecker. The images were then cropped to a size of 150 × 150 pixels. This was the maximum size the images could be as the objects appear quite small when imaged from 70°. Images of the samples were used rather than the samples themselves for two reasons. First, it was much faster for observers to make image comparisons than to readjust the physical samples while maintaining a constant angle of observations. Second, using images allowed observers to compare two angles of the same sample simultaneously rather than readjusting the samples and making judgments from memory.

The experimental graphical user interface (GUI), shown in Figure 6, was built and run using MATLAB 2018b software, which was also used to record observer responses. Images were shown to observers on an Ezio® ColorEdge CG238 calibrated display. In a two-alternative forced choice experiment, observers were shown the same print from two different angles and asked to select the image that appeared greener. There were 15 observers with a total of 15 angles to compare (−70° to 70°) for each of the three 3D printed samples. Observations were made in a dark room and each observation session took approximately 15 minutes, so observer fatigue was not a factor. In this experiment, there was no delay between the images shown. In future work, a neutral image will be used to reduce observer after-image effects. A Thurstonian analysis of the paired comparisons was used to place observations on an interval scale of "green" appearance [18]. The resulting scale values are not an absolute measure of green but rather a measure of relative color perception when viewing the printed objects at different angles. The greener an object appeared at a given angle, the greater its scale value.

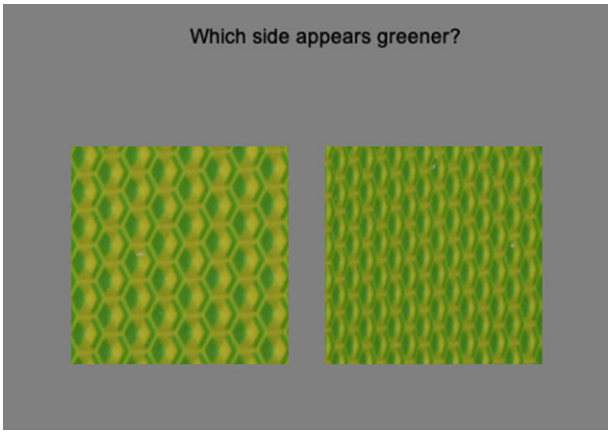

Figure 6. Screenshot of GUI used in the experiment.

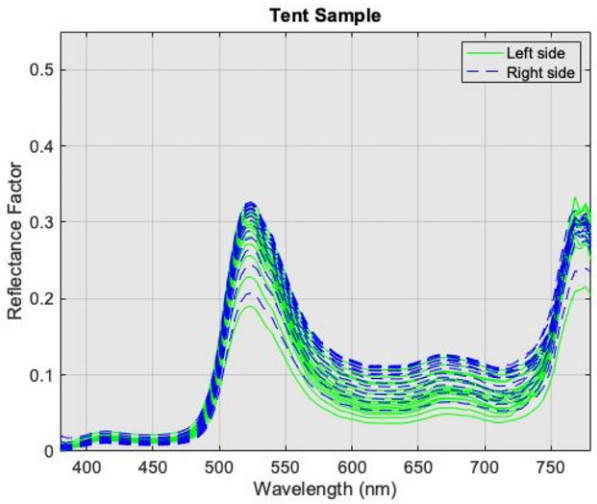

Figure 7. Reflectance factor for the tent sample.

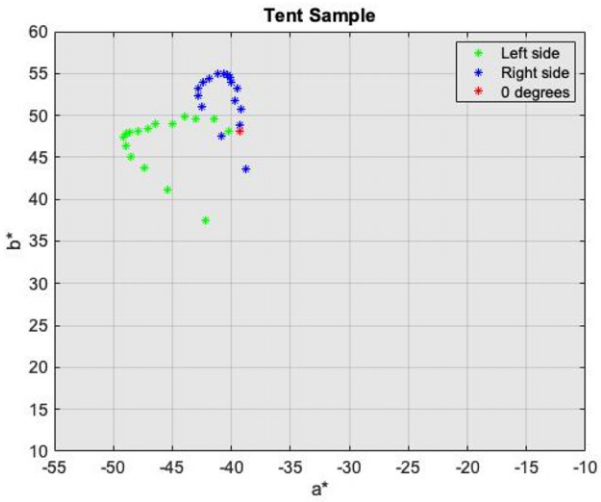

Figure 8. a^*b^*coordinates for the tent sample.

3. RESULTS

3.1 *Measurements*

The radiance measured from the samples and the radiance measured from a perfect reflecting diffuser were used to calculate reflectance factor for each sample at each angle, as seen in Figure 7. The reflectance factor was then used to calculate the CIE XYZ tristimulus values as well as CIELAB values (Figures 8–10) [7, 16].

What is important to note here is the divergence in the shape of the tent and honeycomb samples when viewing them from either the left or right side, and the lack of divergence in the pyramid sample. The honeycomb and pyramid samples show some extremes outside the clustered measurements. This is due to some specular highlights on the samples near the smaller angles, ∼10° from surface normal, which was likely due to the clear coat finish applied by the manufacturer. The finish was applied to each of the samples, so it is curious that this did not occur with the

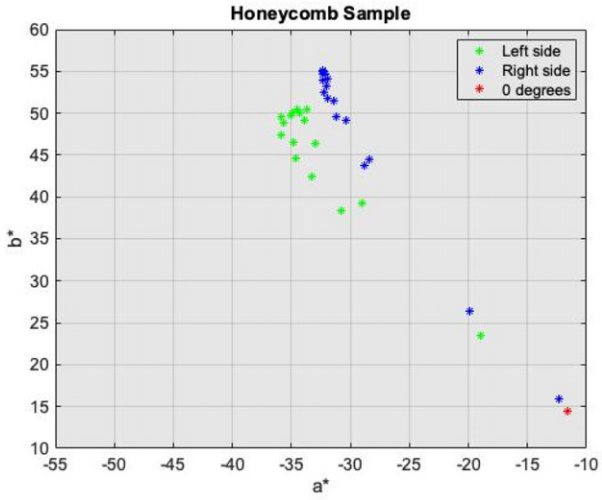

Figure 9. a^*b^* coordinates for the honeycomb sample.

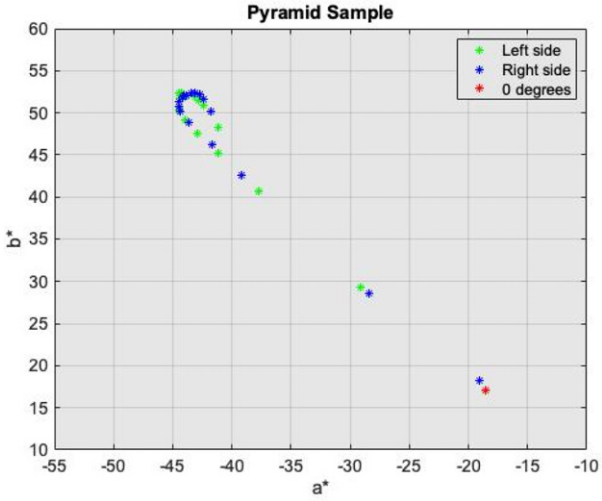

Figure 10. a^*b^* coordinates for the pyramid sample.

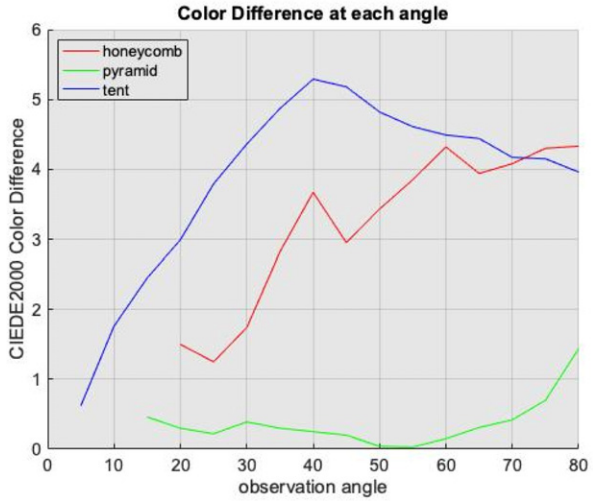

Figure 11. CIEDE2000 color differences calculated for equal angles between 5° and 80° on either side of the samples.

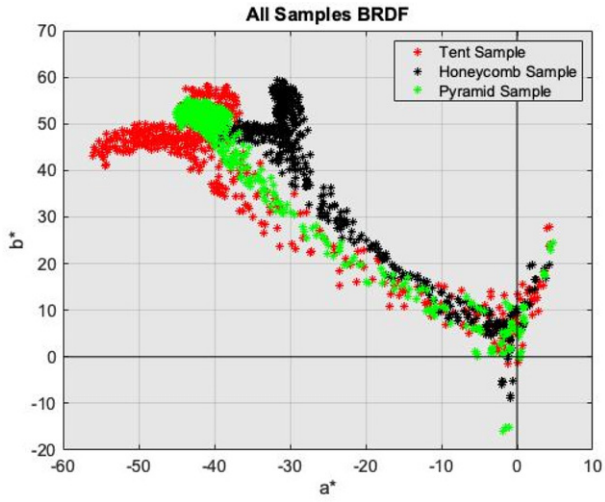

Figure 12. Calculated a^*b^* values for all three samples.

tent sample and will require further investigation. L^* values were similar, ∼40–50, for all samples at all angles, with the exceptions being near the center for the pyramid and honeycomb samples where specular highlights appeared.

The color differences were calculated for equal but opposite angles of observation measurements on both sides of the samples. For example, the difference between 5° to the left of the sample's surface normal was compared to 5° to the right. Looking at the tent sample in Figure 11, the largest measured difference from an angle on one side of surface normal when compared to the other side of surface normal was found at 40°, resulting in a peak at that angle. This was done for each angle measured. Due to the specular highlights on the honeycomb and pyramid samples, the color differences near those angles have been excluded from Fig. 11 as they are not helpful here.

Figure 12 shows the plotted a^*b^* values of the three samples. Measurements were taken by rotating the samples within the goniospectrophotometer, changing the angle of observation. The angle of incident light was varied independently as well. A similar divergence previously observed in the measurements taken with the gonio-arm setup can be seen here for the tent and honeycomb samples. This divergence indicates a color shift from yellow–green to grayish to green–yellow as the angles of observation shifts along the face of the samples. The grayish colors here occur as the observation angle approaches the specular highlights. Again, no apparent divergence was observed for the pyramid sample.

3.2 *Visual Experiment Results*

For both the tent and the honeycomb samples, one side is clearly observed to be greener, indicated by higher interval scale values on one side than the other and the lowest point on the "greenness" scale occurring to the negative side of perpendicularity. The pyramid sample shows more symmetry across all angles, indicating that neither side appeared more or less green. This trend matches the measurement data as there is no observed split in the

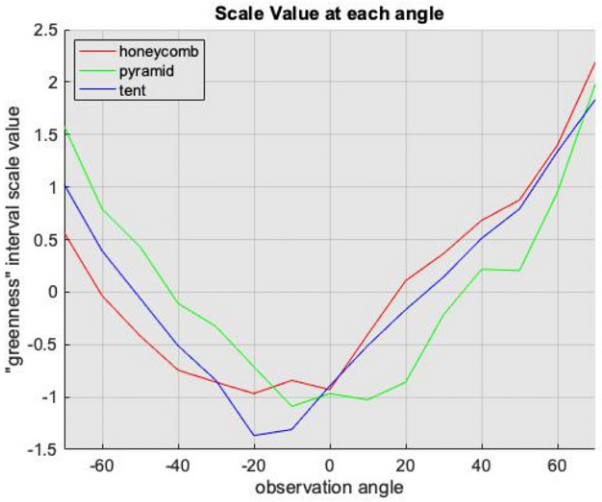

Figure 13. Interval "greenness" scale values for each of the 3D printed samples.

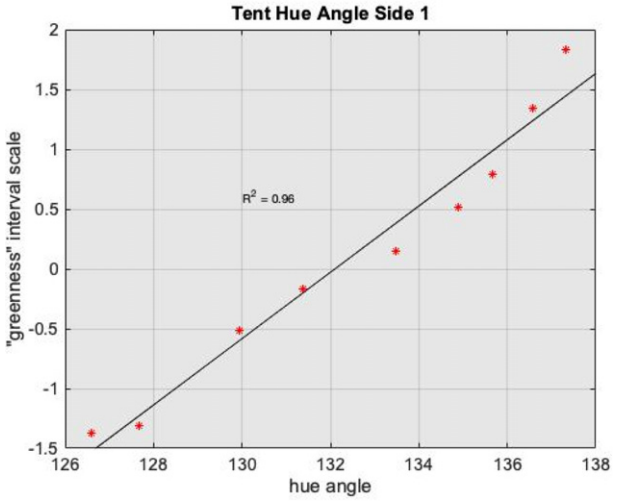

Figure 15. Correlation between the hue angle and the greenness scale value for the tent sample shown for only one side.

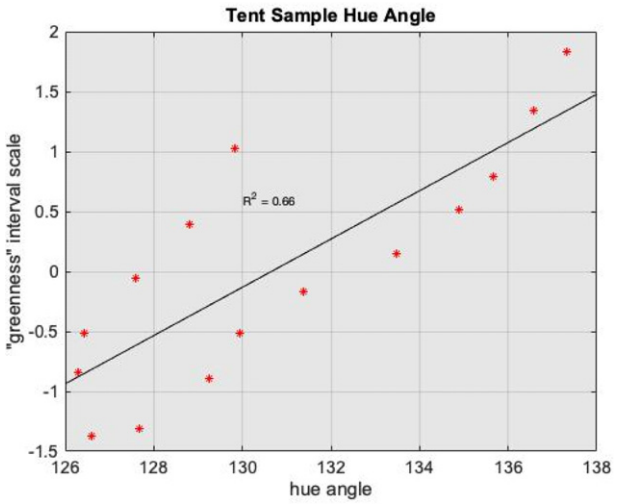

Figure 14. Correlation between the hue angle and the greenness scale value for the tent sample.

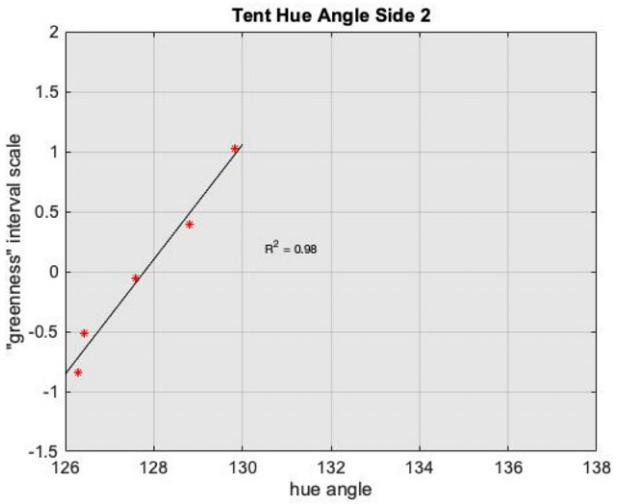

Figure 16. Correlation between the hue angle and the greenness scale value for the tent sample shown for the side opposite to that in Fig. 15.

pyramid measurements, while the others show a well-defined divergence in a^* and b^*, as seen in Fig. 12.

There is some correlation between the hue angle and the greenness scale value in the tent sample when all observation angles are considered (Figure 14). Note, however, the appearance of two separate lines in this graph. These represent the two sides of the tent sample.

For the pyramid and honeycomb samples, the minimum greenness scale value was at 0°, as seen in Figure 13, though the tent sample's minimum was at −20°. As with Fig. 11, the specular highlights were removed from the pyramid and honeycomb plots as they could not be meaningfully correlated. When each side from the point seen as the least green is considered separately, Figures 15–20, the correlation between the measured hue angle and the observed greenness is much stronger in most cases. The lone exception is one side of the honeycomb sample, seen in Figure 18. This is the "yellower" side of the honeycomb. Its value of greenness may be impacted by spatial features that are on a scale that is too small to measure with its color appearance because its scale value still increases as it moves farther from surface normal, as seen in Fig. 13. In other words, it is still being perceived as more green at more extreme viewing angles despite the inconsistent changes in the hue angle. This is likely caused by the relatively small scale on which these hue angles lie, with a maximum difference of only ∼1.5°.

4. DISCUSSION

The color 3D printed samples did produce measurable goniochromatic effects which were visible to human observers. The samples printed with different 3D geometries produced CIELAB values that were quite different despite using the same colored material, suggesting that manipulating the geometries of color 3D printed objects on a small scale does offer some level of control on the object's appearance.

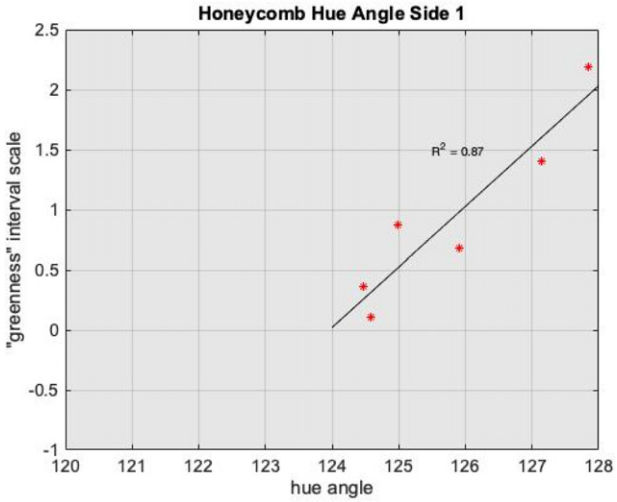

Figure 17. Correlation between the hue angle and the greenness scale value for the honey sample shown for only one side.

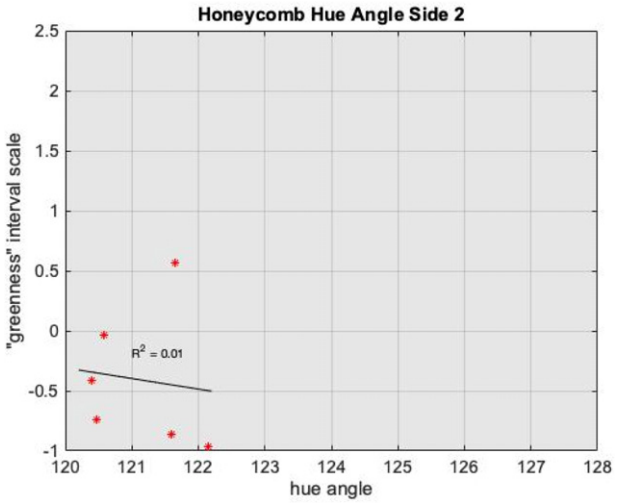

Figure 18. Correlation between the hue angle and the greenness scale value for the honeycomb sample shown for the side opposite to that in Figure 17.

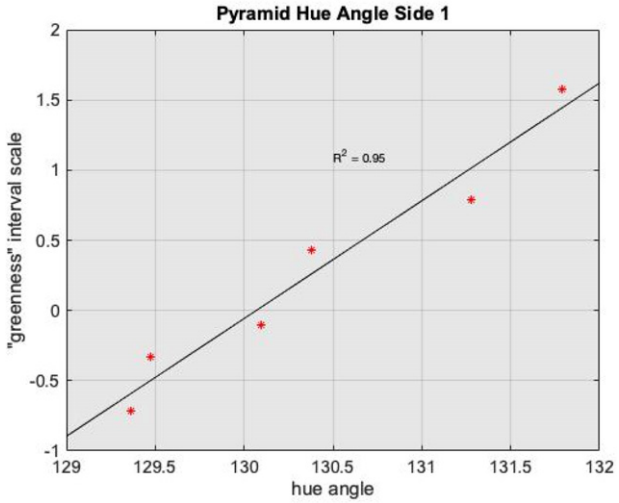

Figure 19. Correlation between the hue angle and the greenness scale value for the pyramid sample shown for only one side.

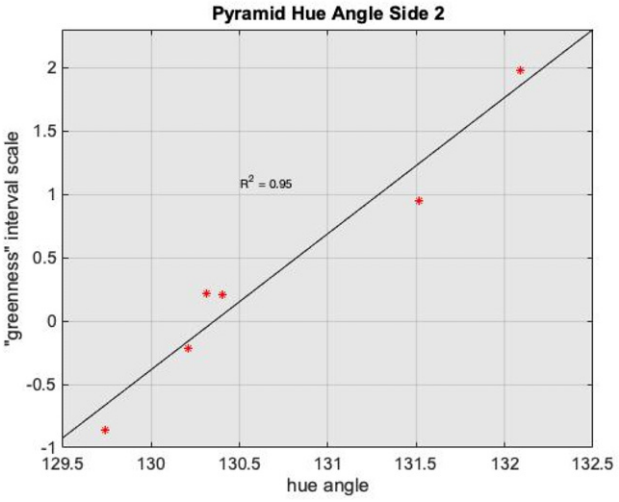

Figure 20. Correlation between the hue angle and the greenness scale value for the pyramid sample shown for the side opposite to that in Figure 19.

The color measurements with both the gonio-arm setup and the goniospectrophotometer indicated a divergence in the hue angle for the tent and honeycomb samples but not the pyramid sample. These measurements were strongly correlated with the results of a psychophysical experiment showing that observers made similar observations when comparing the samples at different angles. The greener the measurements were at each angle, the greener the observers judged the samples to be at that same angle. It is important to note that there are several points where the hue angle from the gonio-arm measurements and the greenness scale values were not consistent. For example, there are two angles shown in Fig. 14, which both have measured hue angles of 130° but have greenness scale values of −0.5 and +1. This may be due to spatial differences in the samples. As the samples are viewed from more extreme angles, the spatial frequency of the geometry will increasingly cause features to appear closer together, as seen in Fig. 6. For the two measured hue angles of 130° mentioned above, one was at −70° and the other at 10°. Although a spectrophotometer may measure the same amount of "green" in a sample at two given angles, this does not guarantee that a human observer will perceive the same color when viewing the sample from those same angles.

REFERENCES

[1] M. J. Domingue, A. Lakhtakia, D. P. Pulsifer, L. P. Hall, J. V. Badding, J. L. Bischof, R. J. Martín-Palma, Z. Imrei, G. Janik, V. C. Mastro, M. Hazen, and T. C. Baker, "Bioreplicated visual features of nanofabricated buprestid beetle decoys evoke stereotypical male mating flights," Proc. Natl. Acad. Sci. **111**, 14106–14111 (2014).

[2] C. W. Hull, "Apparatus for production of three-dimensional objects by stereolithography," US Patent No. 4,575,330 (1986).

[3] J. Yuan, M. Zhu, B. Xu, and G. Chen, "Review on processes and color quality evaluation of color 3D printing," Rapid Prototyping J. **24**, 409–415 (2018).

[4] A. Brunton, A. A. Can, and P. Urban, "Pushing the limits of 3D color printing: Error diffusion with translucent materials," ACM Trans. Graph. **35**, 4 (2015).

[5] V. Babaei, K. Vidimče, M. Foshey, A. Kaspar, P. Didyk, and W. Matusik, "Color contoning for 3D printing," ACM Trans. Graph. **36**, 124 (2017).

[6] C. Parraman, "Methods for multi-layer color printing and decorative inks for ultra-violet fine art inkjet," J. Imaging Sci. Technol. **57**, 40503-1 (2013).

[7] R. S. Berns, *Billmeyer and Saltzman's Principles of Color Technology* (Wiley, Hoboken, NJ, 2019).

[8] M. Derhak, P. Green, and T. Lianza, "Introducing iccMAX: new frontiers in color management," Proc. SPIE **9395** (2015).

[9] W. Hung and P. Sun, "BRDF measurement and color appearance simulation based on iccMAX framework," *ICC Meeting on Display and 3D Printing* (International Color Consortium, Taipei, Taiwan, 2016).

[10] P. Sun and Y. Sie, "Color uniformity improvement for an inkjet color 3D printing system," *IS&T Electronic Imaging: Color Imaging XXI: Displaying, Processing, Hardcopy, and Applications* (IS&T, Springfield, VA, 2016), pp. 1–6.

[11] S. K. Shevell and F. A. A. Kingdom, "Color in complex scenes," Annu. Rev. Psychol. **59**, 143–166 (2008).

[12] Stratasys 2019 *J735 and J750*. Retrieved March 6, 2019, from https://www.stratasys.com/3d-printers/j735-j750.

[13] R. Singh, "Process capability study of polyjet printing for plastic components," J. Mech. Sci. Technol. **25**, 1011–1015 (2011).

[14] M. Ronnenberg and S. P. Farnand, "The effect of surface texture on color appearance of 3D printed objects," *Proc. IS&T CIC26: Twenty-Sixth Color and Imaging Conf.* (IS&T, Springfield, VA, 2018), pp. 128–133.

[15] Polyjet Color Materials Guide, received from Stratasys® Direct Manufacturing via email on 10/30/2017.

[16] R. W. G. Hunt and M. R. Pointer, *Measuring Colour* (John Wiley & Sons, Hoboken, NJ, 2011).

[17] G. A. Gescheider, *Psychophysics: Method, Theory, and Application* (Lawrence Erlbaum, Mahwah, NJ, 1985).

[18] L. L. Thurstone, "A law of comparative judgment," Psychological Rev. **34**, 273 (1927).